Microsystem Technologies 10 (2004) 412–418 © Springer-Verlag 2004
DOI 10.1007/s00542-004-0444-x

Fracture behaviour of single crystal silicon microstructures

F. Favalli Meroni, E. Mazza

Abstract The fracture behaviour of single crystal silicon (SCSi) microstructures is analysed based on micromechanical torsional and tensile experiments. The uniaxial testpieces are characterised by the presence of sharp notches at the gauge length extremities. The critical loading conditions are reproduced in a finite element model in order to identify the analogies of the failure conditions in tension and torsion. The stress field in the vicinity of the notch tip (were cracks originate) is analyzed, and fracture mechanics parameters are determined. In the finite element model a crack, reproducing the failure process observed in the experiments, is included. The crack area is incrementally increased and the energy release rate for the critical loading conditions in tension and torsion is calculated. Based on these results a failure criterion is formulated along with a procedure for the mechanical integrity analysis of SCSi microstructures of arbitrary shape and loading conditions.

1 Introduction

Single Crystal Silicon (SCSi) is widely applied for the realization of micromechanical devices, such as pressure sensors, accelerometers, micropumps and micromotors. The deformation analysis of a SCSi microstructure for a given mechanical load or the calculation of its resonance frequencies does not present any particular problem. In fact, the constitutive behaviour of micromachined SCSi has been characterized in a number of micromechanical tests aiming at determining its elastic constants [1–7]. On the other hand, failure criteria and viable calculation procedures for the mechanical integrity analysis of SCSi microstructures are still missing, despite the availability of a certain amount of strength data [3, 5, 6, 8–11]. The definition of design criteria and practicable calculation procedures represents an essential step towards the realization of reliable and optimized SCSi microstructures.

Due to its brittleness, SCSi experiences sudden fracture and catastrophic failure when the mechanical load on the microstructure exceeds a critical value. In most cases failure originates at stress risers (notches) generated by the micromachining techniques, such as chemical etching, ion reaction etching or plasma etching. In the case of anisotropic chemical etching the stress field is singular along the sharp notches formed by the intersection of different etching planes.

One possible design procedure is the classical strength analysis, in which a representative stress value is compared with the appropriate strength limit of the material. The definition of the representative stress value (as function of the tensor components) and the determination of the strength limit represent difficult tasks in the case of a brittle anisotropic material [12]. To the knowledge of the authors, these tasks have not been accomplished so far. In the opinion of the authors, this approach deserves further consideration in future studies. In the present work a fracture mechanics based approach has been favoured.

Design based on fracture mechanics is suitable for an intrinsically brittle material, such as SCSi. Fracture mechanics parameters have been applied by several researchers for the definition of the critical loading conditions in SCSi [7, 12, 13]. In particular, fracture mechanics is the only viable approach for the analysis of microstructures with atomically sharp notches, due to the singularity of the stress field at the notch tip.

In [7, 12] stress intensity factors are calculated for particular loading conditions at sharp notches in SCSi microstructures. The calculations are based on mixed analytical-numerical analysis of the stress near field at the notch tip. The design criteria proposed in these works suffer of important limitations, since they only apply for specific notch geometry and loading conditions.

An attempt for the derivation of a failure criterion of general validity is presented in [5]. There, experiments with microbeams subjected to tensile load are described and a failure criterion is formulated based on the comparison between the energy density in the notch near-tip region and the surface energy per unit area. In a successive paper [6], torsional tests with the same micromechanical test pieces are presented. The application of the failure criterion proposed in [5] for the experimental data of [6] confirmed to some extent the validity of the approach, though highlighted the necessity of improving the formulation for the criterion to hold general validity.

The experimental data from [5] and [6] are analysed and compared in the present work, with the aim of defining a failure criterion of general validity and a guideline for the strength analysis of SCSi micromechanical structures.

Received: 18 June 2003 / Accepted: 12 November 2003

F. Favalli Meroni, E. Mazza (✉)
Institute of Mechanical Systems,
ETH Zürich, 8092 Zürich, Switzerland
e-mail: mazza@imes.mavt.ethz.ch

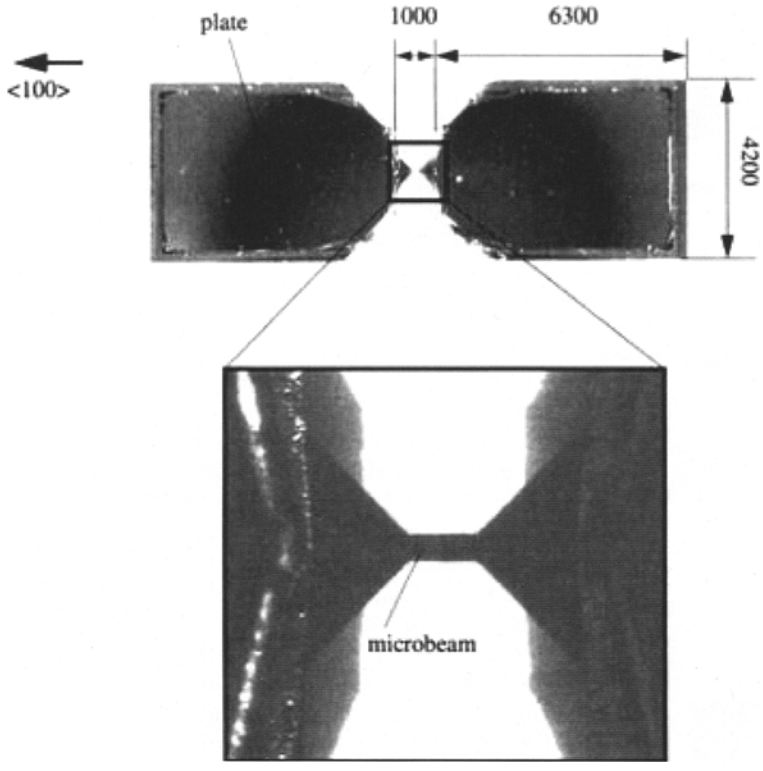

Fig. 1. SCSi sample used in this study with a magnification of the microbeam (dimensions in micrometer)

2
Material, specimens and experimental conditions

Micromechanical tensile tests are presented in [5] and torsional tests in [6]. In both cases SCSi with a low level of doping inclusions (p-type, resistivity: 3.0÷3.5 Ω/cm) is used. Specimens are realized by KOH etching of {100} silicon wafers. Details on the fabrication process are given in [5]. The specimens consist of two plates ($6.3 \times 4.2 \times 0.38$ mm^3) connected by a microbridge (the actual testing region, Fig. 1). The testing region presents at its extremity sharp notches due to the fabrication process.

The dimensions of the specimens vary in the ranges indicated in Fig. 2.

When an external load is applied to the specimens (tensile force or torque) a stress distribution is generated in the microstructure, with strong stress concentrations around the notches at the gauge length extremities (Fig. 3). In all experiments the onset of the fracturing crack occurs in these zones. The critical location changes between tension and torsional tests, but is always located along the notches. Tensile load leads to a stress concentration with maximum at one extremity of the notch line, whereas torsional load leads to a maximum in the middle of the same edge (Fig. 3).

Since the specimens' material is nearly a perfect crystal and the limited extension of the critical zone statistically lessen the probability of a defect at the critical location, a high repeatability of the critical load values is expected [10]. This is confirmed to a great extent by the tensile tests and to a lesser extent by torsional tests. This difference is due to the experimental errors, which are inherently larger in torsional tests compared to the simpler tensile tests [6].

From the results of these experiments the critical load and deformation, just before fracture, can be inferred.

3
FEM Calculations and fracture mechanics Analysis

3.1
FEM model

The FEM calculations are performed with the software ABAQUS 6.2 [14]. The FEM model used to simulate the

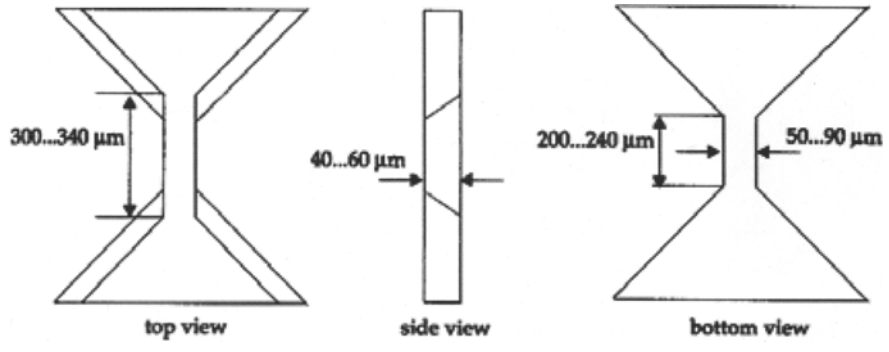

Fig. 2. Geometry of the microbeam

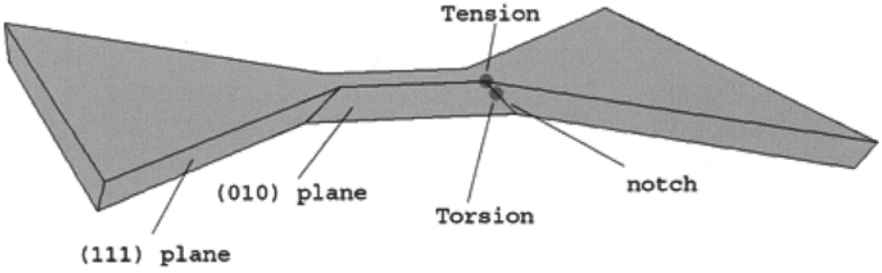

Fig. 3. Different maximum stress concentration points for tensile and torsional test

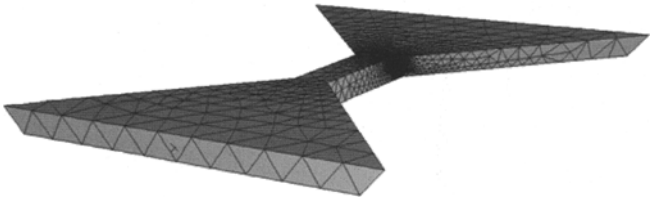

Fig. 4. The FEM model used in simulations

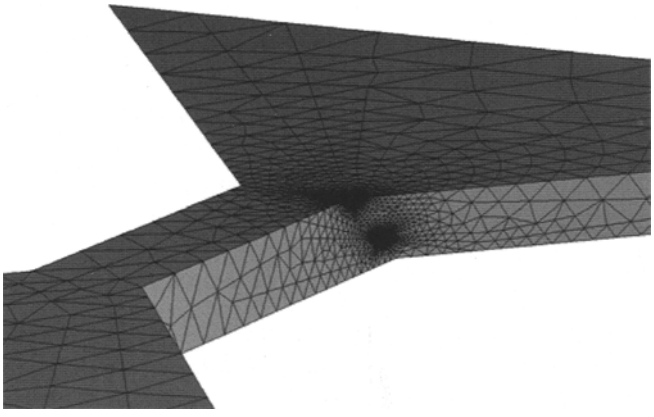

Fig. 5. The strong mesh refinement at the two stress concentration points

critical conditions is shown in Fig. 4. The whole testing region is included in the model. Quadratic tetrahedral elements are used. The mesh refinement at the critical locations for tensile force and torque is shown in Fig. 5.

The simulation of the critical loading conditions at an ideally sharp notch with a linear elastic stress calculation leads to a singularity of the stress field. The singularity can be avoided with a non-linear continuum mechanics calculation (with the equilibrium conditions verified at the deformed configuration, see e.g. [15]). For this, a strong mesh refinement is required at the notch tip in a 3D FEM calculation, leading to very large number of degrees of freedom in the model. Fracture mechanics parameters in the vicinity of the notch tip are evaluated in this work, thus limiting the requirements of mesh refinement.

After some standardization step due to the differences of the geometry of each single specimen tested, the values of the ultimate loads before the catastrophic failure, to be applied as statical boundary condition in the FE simulation, are obtained from the experiments. These are (i) the critical tensile force, F_{crit}, for the tensile tests, and (ii) the critical torque, T_{crit}, for the torsional tests.

The tests are simulated by prescribing the position of the nodes at the extremities of the model: one extremity is always clamped and the other one is moved in the axial direction for tensile tests and twisted for torsional tests. These boundary conditions are coherent with the assumption of rigidity of the two rectangular plates (Fig. 1).

3.2 Fracture mechanics analysis

The fracture mechanics analysis is based on Griffith's theory [16]. Griffith's energy balance for an incremental increase of the crack area dA states that under equilibrium conditions:

$$\frac{dU}{dA} = \frac{dE}{dA} + \frac{dW_s}{dA} = 0 \qquad (1)$$

or

$$-\frac{dE}{dA} = \frac{dW_s}{dA} \qquad (2)$$

where dU is the variation of the total energy of the system, dE is the change in potential energy (variation of internal strain energy and potential of the external forces), dW_s is the work required to create new infinitesimal surfaces of area dA (increment of crack area).

$-dE/dA$ is also called *energy release rate* G, which is a measure of the energy available for an incremental crack extension.

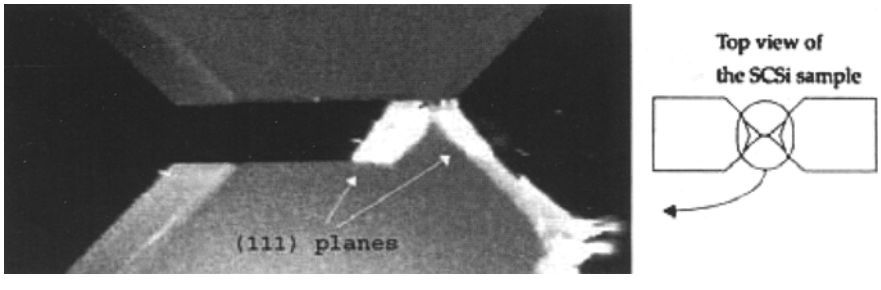

Fig. 6. Fractured specimen after the tensile tests

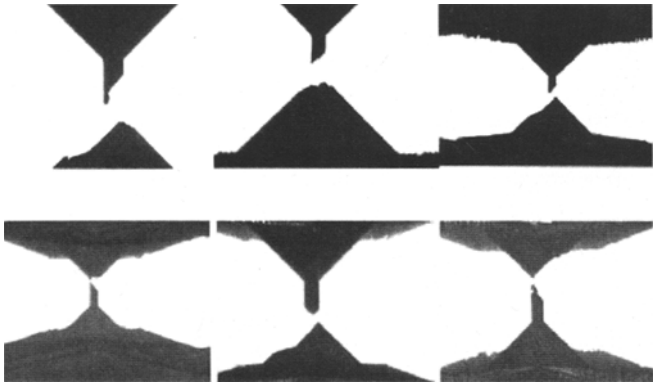

Fig. 7. Fractured specimen after the torsional tests (from [6])

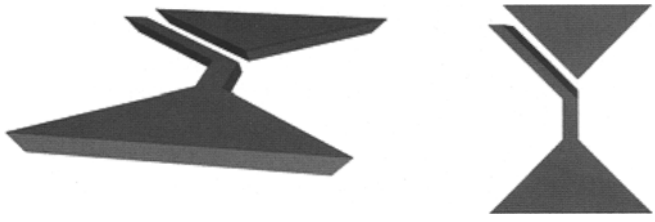

Fig. 8. The plane selected as propagation plane for cracks

The comparison of the energy release rate G with the appropriate surface energy value represents a standard method for evaluating the behaviour of a crack in a solid. The main problem in the present case is that before failure no crack is present in the structure. Thus, a potential cleavage crack has to be identified, for which the energy release rate values are calculated. The aim of this calculation is to reproduce the real fracture process occurring in the experiments and characterize the onset of the crack in tension and torsion by a criterion based on the energy release rate.

The crack is introduced in the FEM model starting from the maximum stress concentration point. Crack opening is simulated by a progressive detachment of adjacent elements at the notch tip. Every step, an incremental increase of the crack area is simulated and the total amount of potential energy is calculated. Interpolating these values, the function $E(A)$ and, from its derivative, the local value of energy release rate $G(A)$ are obtained.

3.3
Crack plane and crack shape

An essential part of this calculation procedure is the determination of the crack plane and the crack shape. The propensity of SCSi to preferential cleavage planes is well known; every macroscopic misalignment from the main planes is supplied by microscopic steps [17], leading to lower values of G. For the identification of the crack propagation plane the cleavage surfaces of broken specimens are analysed: tensile tests show a bifurcating crack running along two {111} planes (see Fig. 6), torsional tests show a wider variety of fracture behaviours, all starting with a {111} plane (see Fig. 7). Since the {111} crystal plane family has the lowest value of surface energy per unit area ($\gamma_{\{111\}} \approx 1.2$ J/m^2, [18, 19]), and according to the experimental observations (see also [11, 20]), cracks are assumed to initiate on {111} planes. Since four {111} planes passes through a single critical point, four cracks, for each loading condition (tension and torsion), propagating along the four {111} planes are evaluated.

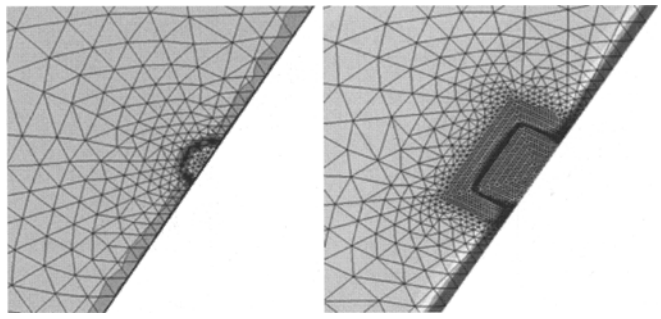

Fig. 10. Stress distribution along the crack front for irregular and regular mesh

For each plane the curve of G(A) in function of the crack area A is calculated. Among the four candidates, the selected plane for crack propagation is determined from the comparison of these curves, searching for the plane with the highest value of energy release. For each loading condition one single plane for the propagation of the crack is identified and further analysis are conducted only on this plane. The crack propagation plane is the same for tensile and torsional test and is shown in Fig. 8.

In the next step, the shape of the crack has to be defined. At the microscopic level the disposition of the atoms in the diamond crystal structure of Silicon (see Fig. 9) allows only a limited range of possible crack fronts. For a crack in the {111} plane, the crack area must be formed by a combination of the triangles shown in Fig. 9. This condition is respected also for the macroscopic cracks in the FEM calculation.

Since cracks are opened in the FEM model by detaching adjacent elements, the shape of the crack strongly depends on the mesh in the refined zone. An irregular mesh pattern leads to irregular shape of the crack. As clearly shown in

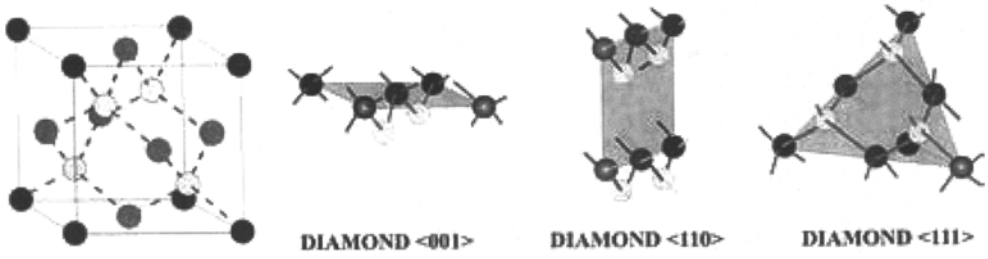

Fig. 9. Diamond structure of SCSi (from [21])

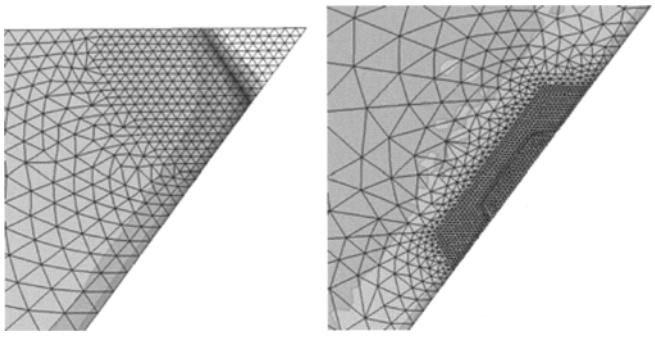

Fig. 11. Crack simulated in tensile tests (left) and torsional tests (right)

Fig. 10, an irregular mesh leads to a significant variation of the stress field along the crack front. With an irregular stress field the energy release rate G is obviously underestimated. A more regular mesh pattern has to be applied in order to obtain a homogeneous stress distribution along the crack front.

Thus the crack shape has to comply with the following requirements:

- uniform distribution of the stress (or strain energy density) along the crack tip line
- compliance also at the macroscopic level with the microscopic crystal structure

The resulting crack shapes for tension and torsion are shown in Fig. 11.

The application of these criteria leads to a crack shape which maximizes the energy release rate G. Thus an unambiguous definition of the crack plane and crack shape for any loading condition and local geometry at the critical location is obtained.

3.4
Energy release rate curves

Potential energy values are evaluated from cracks propagating within the so called near-field region of the notch. These data are then interpolated using a power law:

$$E(A) = a_1 A^{n1} + a_2 A^{n2} \tag{3}$$

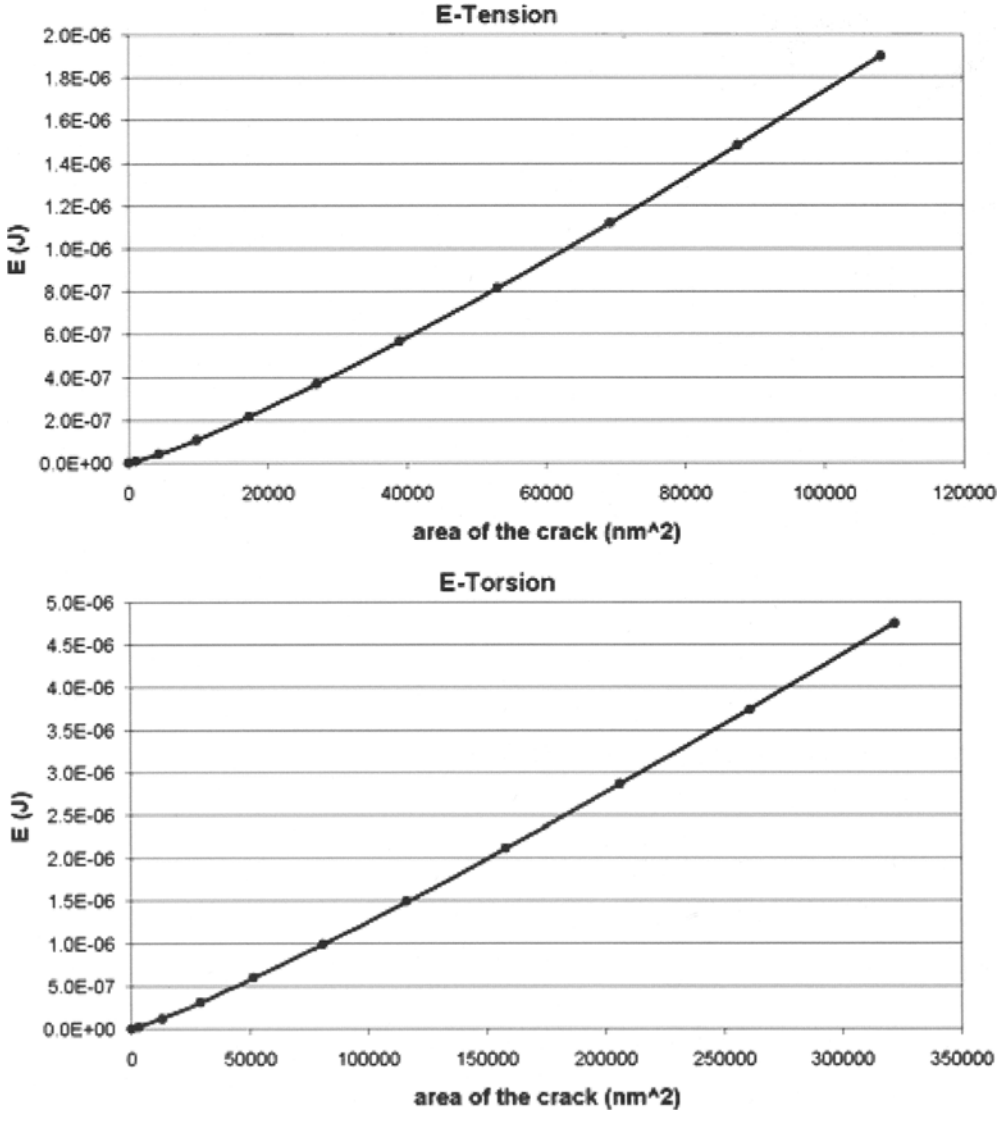

Fig. 12. Interpolation curves (lines) compared with simulated data (points)

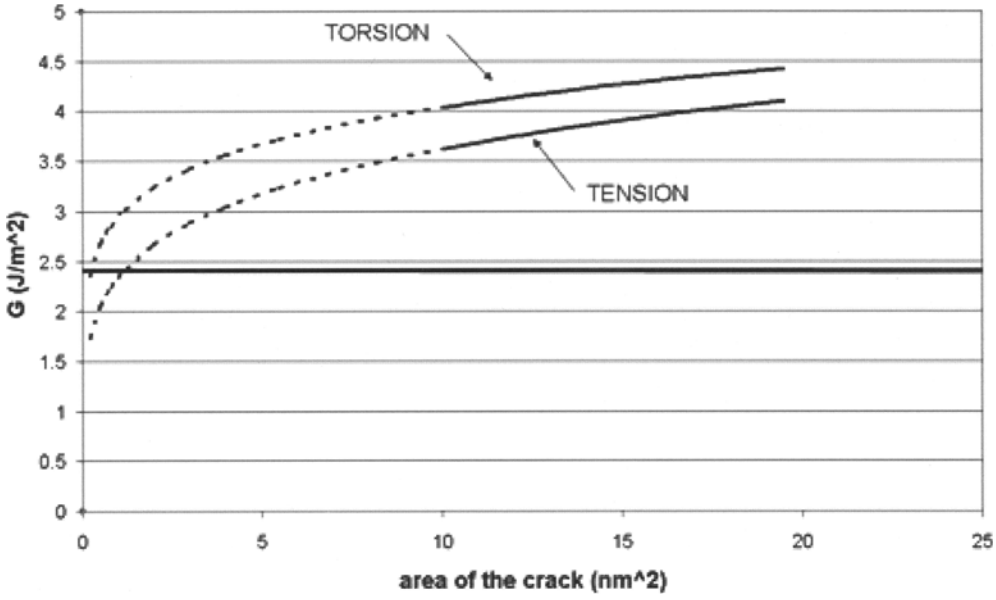

Fig. 13. G curves for tensile and torsional tests in function of the area of the crack

This choice is dictated by the fact that the stress variation in the near field region is described by a power law, [5, 22, 23]. The simulation results are very well fitted with the power law, as shown in Fig. 12 for tensile and torsional tests.

From the function $E(A)$ the energy release rate $G(A)$ is calculated. Fig. 13 shows the function $G(A)$ extrapolated for crack areas in the nm range. The curves for tensile and torsional tests are similar in their shape and in the numerical values, confirming that the function $G(A)$ characterizes the notch at critical loading conditions. Thus a criterion with general validity can be formulated based on these curves.

3.5 Failure criterion

Crack initiation is expected to be governed by the value of the function $G(A)$ for areas in the atomic range ($A \approx 0.25$ nm^2). The curve $G(A)$ calculated according to the procedure presented above is expected to hold validity down to a crack area of 10 nm^2. Below this value, the validity of the near field solution is questionable due to a number of factors, such as the exact geometry of the notch tip (influenced by the surface roughness, in the range of 1 nm, [11, 24]) or the geometrical non-linearity due to the large values of strains (up to 5% at 3 nm from the notch tip). These factors are all expected to reduce the value of the function $G(A)$. Therefore the evaluation of the value of the curve $G(A)$ for $A = 10$ nm^2 leads an upper bound for the energy release rate at the atomic level. The following (conservative) failure criterion can therefore be formulated: fracture originates if $G(A = 10\ \text{nm}^2)$ exceeds the surface energy required to form two new {111} faces ($2\gamma = 2.4$ J/m^2):

$$G(A = 10\ \text{nm}^2)_{\text{crit}} = 2.4\ \text{J/m}^2 \qquad (4)$$

Correspondingly, for tensile and for torsional test lower values would have been predicted by this criterion for the critical load than the measured ones. As depicted in Figure 14, with the above criterion the load would have been limited to a 22% lower tensile force and 29% lower torque in tension and torsional test respectively. The

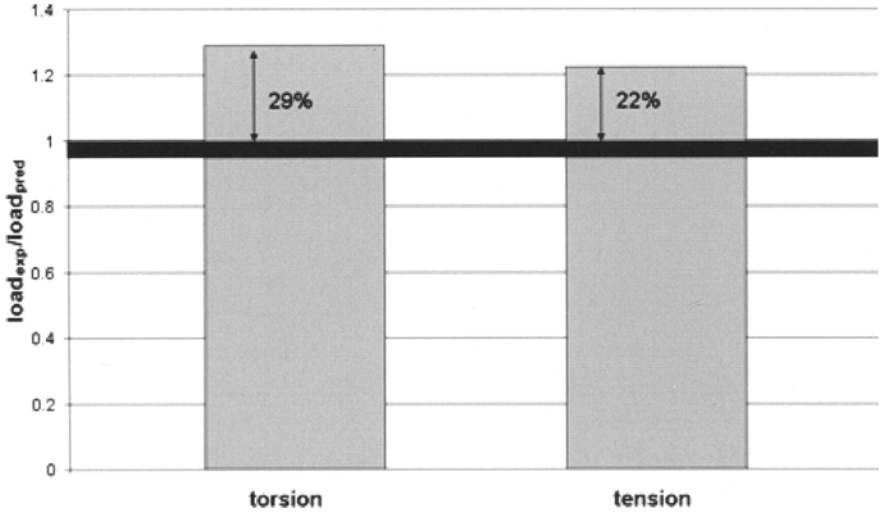

Fig. 14. Comparison of measured and predicted critical loads, according to the failure criterion, Eq. (4)

conservatism is the consequences of the significant level of uncertainty related to mechanical behaviour at the atomic level in the vicinity of the notch tip.

4 Conclusions

The design procedure presented in this paper can be applied to any SCSi structure subjected to arbitrary loading conditions. It mainly consists of four steps: (i) identify the critical location (with a global model, coarse mesh); (ii) identify the crack plane (among the four {111} planes passing through the critical point, with a refined, but still relatively coarse mesh); (iii) calculate for the critical plane the curve G(A), applying a crack shape which satisfy specific criteria (for this step a refined mesh is required); (iv) evaluate the value G(A = 10 nm^2) and compare with G(A = 10 nm^2)$_{crit}$.

This method provides a baseline for a conservative evaluation of the strength of a SCSi microstructure. Future work will concentrate on the verification of the failure criterion for different geometries and loading conditions. For this purpose, bending tests with SCSi probes with notches of different wedge angle will be performed. As well a validation of this approach will be attempted by its direct application to strength data from the literature. This work will help quantifying (and possibly reducing) the inherent level of conservatism of the design procedure presented in this paper.

References

1. **Hok B; Gustafsson K** (1985) Vibration analysis of micromechanical elements. Sensors Actuators 8:235–243
2. **Weihs TP; Hong S; Bravman JC; Nix WD** (1988) Mechanical deflection of cantilever microbeams - a new technique for testing the mechanical-properties of thin-films. J Mater Res 3:931–942
3. **Johansson S; Ericson F; Schweitz JA** (1989) Influence of surface-coatings on elasticity, residual-stresses, and fracture properties of silicon microelements. J Appl Phys 65:122–128
4. **Schweitz JA** (1992) Mechanical characterization of thin-films by micromechanical techniques. Mrs Bulletin 17:34–45
5. **Mazza E; Dual J** (1999) Mechanical behavior of a mu m-sized single crystal silicon structure with sharp notches. J Mech Phys Solids 47:1795–1821
6. **Schiltges G; Dual J** (2001) Failure behaviour of microstructures under torsional loads. J Mech Phys Solids 49:1021–1038
7. **Wan SW; Dunn ML; Cunningham SJ; Read DT** (1999) Elastic moduli, strength, and fracture initiation at sharp notches in etched single crystal silicon microstructures. J Appl Phys 85:3519–3534
8. **Pearson GL; Read WT; Feldmann WL** (1957) Deformation and fracture of small silicon crystals. Acta Metallurgica 5:181–191
9. **Yi T; Kim CJ** (1999) Measurement of mechanical properties for MEMS materials. Meas Sci Technol 10:706–716
10. **Namazu T; Isono Y; Tanaka T** (2000) Evaluation of size effect on mechanical properties of single crystal silicon by nanoscale bending test using AFM. J Microelectromechanical Syst 9:450–459
11. **Sundararajan S; Bhushan B; Namazu T; Isono Y** (2002) Mechanical property measurements of nanoscale structures using an atomic force microscope. *Ultramicroscopy* 91:111–118
12. **Suwito W; Dunn ML; Cunningham SJ** (1998) Fracture initiation at sharp notches in single crystal silicon. J Appl Phys 83:3574–3582
13. **Fett T** Failure of brittle materials near stress singularities. (1996) Engineering fracture Mechanics 53:511–518
14. ABAQUS Theory Manual, Version 6.2 edn. (2001) Hibbitt, Karlsson & Sorensen, Inc.
15. **Seweryn A** (2002) Modeling of singular stress fields using finite element method. Int J Solids Struct 39:4787–4804
16. **Griffith AA** (1968) Phenomena of rupture and flow in solids. Asm Trans Q 61:871
17. **Haneman D** (1987) Surfaces of silicon. Rep Prog Phys 50:1045–1086
18. **Gilman JJ** (1960) Direct measurements of the surface energies of crystals. J Appl Phys 31:2208–2218
19. **Messmer C; Bilello JC;** (1981) The surface-energy of Si, Gaas, and Gap. J Appl Phys 52:4623–4629
20. **Enzler A; Herres N; Dommann A** (2002) Analysis of etched cantilevers. Microelectronics Reliability 42:1807–1809
21. **Elwenspoek M; Jansen HV** (1998) Silicon Micromachining. Cambridge: Cambridge University Press
22. **Williams ML** (1952) Stress singularities resulting from various boundary conditions in angular corners of plates in extension. J Appl Mech-Trans Asme 19:526–528
23. **Stroh AN** (1962) Steady state problems in anisotropic elasticity. J Math Phys 41:77
24. **Findler G; Muchow J; Koch M; Munzel H** (1992) Temporal evolution of silicon surface-roughness during anisotropic etching processes presented at Ieee Micro Electro Mechanical Systems : An Investigation of Micro Structures, Sensors, Actuators, Machines and Robots, New York